A Level Set Finite Element Anisotropic Grain Growth Study

Julien Fausty, Nathalie Bozzolo, Marc Bernacki

A Level Set Finite Element Anisotropic Grain Growth Study

Julien Fausty, Nathalie Bozzolo and Marc Bernacki

MINES ParisTech, PSL - Research University, CEMEF - Centre de mise en forme des matériaux, CNRS UMR 7635, CS 10207 rue Claude Daunesse, 06904 Sophia Antipolis Cedex, France

Application

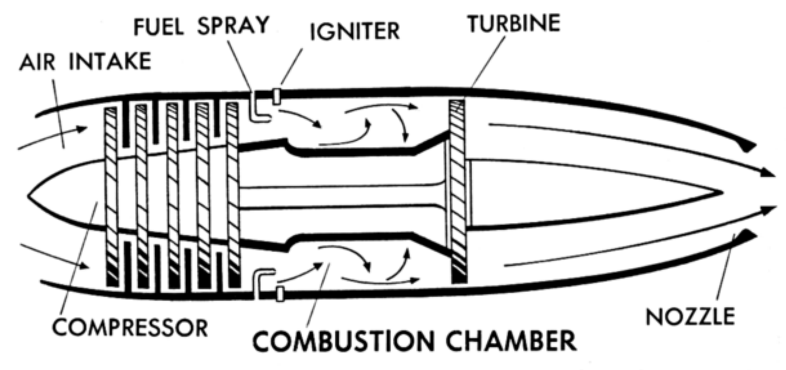

Fig. 1: A diagram of an generic aircraft engine.

The turbine disks of aircraft engines, obtained by hot forging, must withstand extreme pressures at extreme temperatures and resist to fatigue crack propagation.

Material

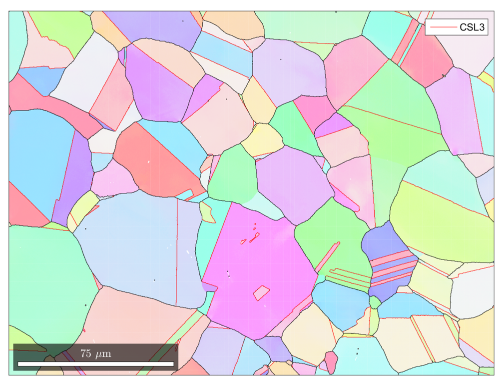

Fig. 2: Experimental EBSD map of an Inconel 718 billet with twin boundaries in red and grain boundaries in black, furnished by Alexis Nicolay.

The material of choice for these disks are often Ni based superalloys whose compositions and microstructures have to be optimized. Annealing twins, boundaries of lower energy, are often present in these microstructures and play an important role in the in-service properties [TCV16].

Numerics

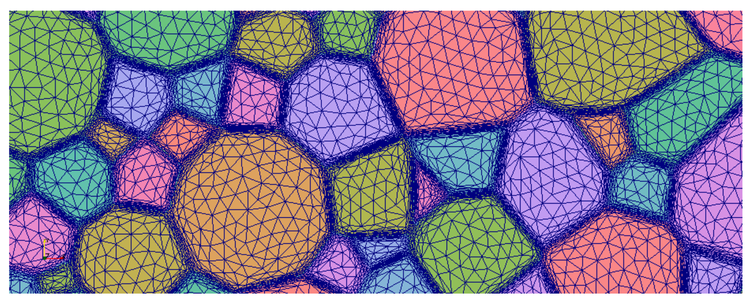

Fig. 3: A part of a numerical microstructure.

To accelerate the material development process, industrial players need numerical tools to simulate microstructural evolutions during forging operations. None of the existing frameworks are able to handle strong anisotropy of grain boundary energy correctly.

Thermodynamics

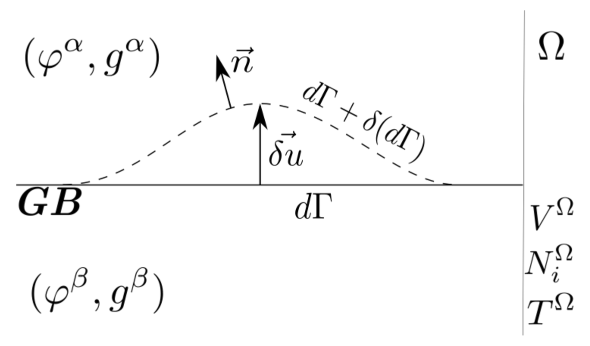

Fig. 4: Schema of the creation of a hump at a grain boundary.

If γ is the grain boundary energy and P_Γ is the pressure felt by the grain boundary. At equilibrium, neglecting the torque terms:

$$P_\Gamma = -\gamma\kappa \tag{1}$$

where κ is the curvature of the grain boundary [Her99]. The velocity of the grain boundary $\vec{v}_n$ is defined as:

$$\vec{v}_n = \mu P_\Gamma \vec{n} \tag{2}$$

where μ is the mobility of the grain boundary and $\vec{n}$ is the unitary normal to the boundary.

LS-FE

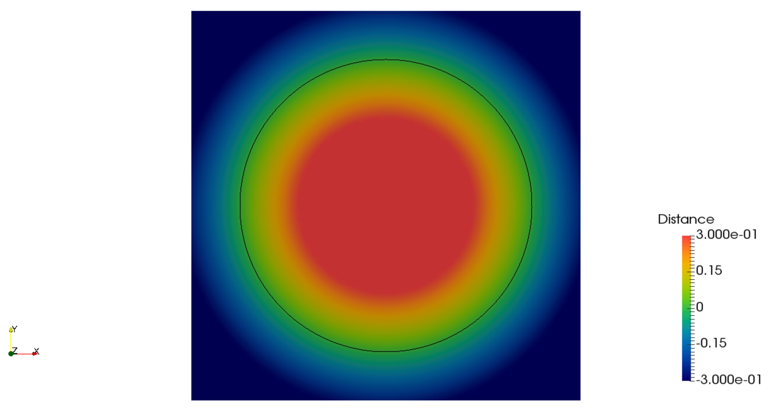

Fig. 5: Le level-set distance function of a circular grain.

The grain boundary network Γ is represented by a set of N signed distance functions such that for $(X,t) \in \Omega \times [0, t_{end}]$ [BLC11]:

$$\left\{ \begin{array}{c} \phi_i(X,t) = \pm d(X,\Gamma) \\ ||\vec{\nabla}\phi_i|| = 1 \end{array} \right\} \quad \forall i \in \{0,...,N\} \tag{3}$$

In order to resolve the grain growth problem, a transport equation is used:

$$\frac{\partial \phi_i}{\partial t} + \vec{v}_n \cdot \vec{\nabla}\phi_i = 0 \tag{4}$$

Anisotropic Adaptation

Extension of the γ field to the entire Ω domain:

$$\begin{array}{ll} \gamma(X,t) = \gamma_{calc}, & \forall X \in \Gamma \\ \Delta\gamma = 0 & \forall X \in \Omega \end{array} \tag{5}$$

using a FE solver.

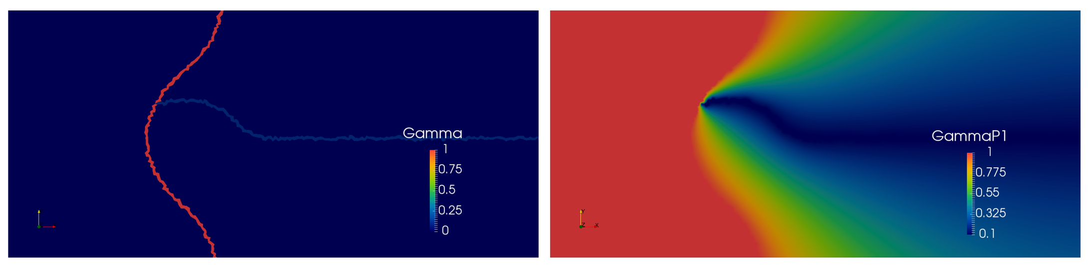

Fig. 6: Before and after an extension operation on γ.

A supplemental convection term due to the weak formulation is taken into account in the anisotropic model using a Convection-Diffusion assembly of the FE matrix. Equation (4) becomes:

$$\frac{\partial \phi_i}{\partial t} - \mu\gamma\Delta\phi_i = 0 \tag{6}$$

with a weak formulation using $\varphi \in H_0^1(\Omega)$ as a test function:

$$\int_\Omega \frac{\partial \phi_i}{\partial t}\varphi + \int_\Omega \mu\vec{\nabla}\gamma \cdot \vec{\nabla}\phi_i \varphi + \int_\Omega \mu\gamma\vec{\nabla}\varphi \cdot \vec{\nabla}\phi_i = 0 \tag{7}$$

The Grim Reaper

In [GNS99] an academic case is described:

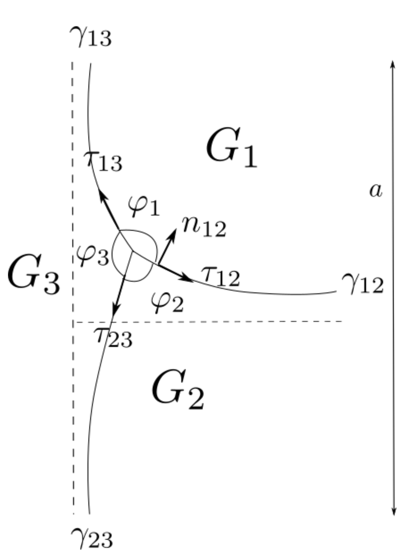

Fig. 7: Diagram of the Grim Reaper case.

If $\gamma_{23} = \gamma_{13}$, the system achieves a stationary state where:

$$\frac{\gamma_{ij}}{\sin\varphi_k} = K \tag{8}$$

$$\cos\frac{\varphi_3}{2} = \frac{\gamma_{23}}{2\gamma_{12}} = \frac{r}{2} \tag{9}$$

$$v_x = \frac{\gamma_{12}\mu(\pi - \varphi_3)}{a} \tag{10}$$

with K a constant.

In this work:

$$\gamma_{23} = 1$$
$$a = 2$$
$$\mu = 1$$

and γ_{12} is varied with r.

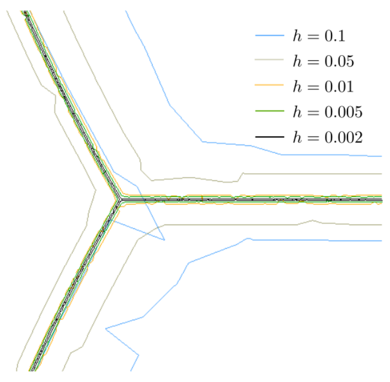

Fig. 8: Zoomed up image of the triple junction at t_{end} for different mesh sizes.

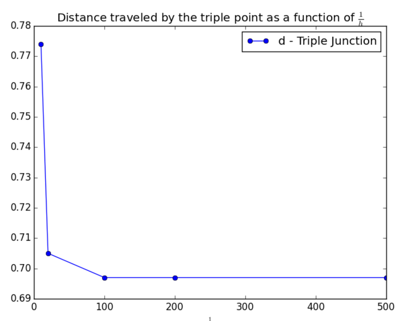

Fig. 9: Graph of the position of the triple junction at t_{end} for different mesh sizes.

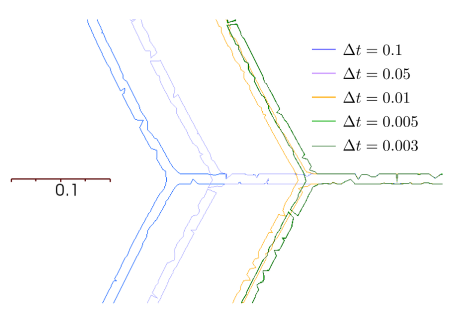

Fig. 10: Zoomed up image of the triple junction at t_{end} for different time steps.

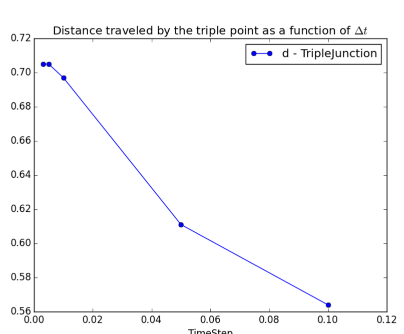

Fig. 11: Graph of the position of the triple junction at t_{end} for different time steps.

Sensibility

h

Mesh size range:

$$h = [0.1\,;\,0.002]$$

with $\Delta t = 0.01$ and $r = 2$.

- P_{tr} used as a convergence criteria.
- Small dependence of the solution with respect to mesh size.
- Convergence is obtained starting at:

$$h = 0.01$$

Δt

Time step range:

$$\Delta t = [0.1\,;\,0.003]$$

with $h = 0.01$ and $r = 2$.

- P_{tr} used as a convergence criteria.
- Large dependence of solution on time step.
- Convergence is obtained for Δt starting at:

$$\Delta t = 0.01$$

The financial support of this work via the industrial Chair OPALE co-financed by SAFRAN and the French National Research Agency (ANR) is acknowledged by the authors.

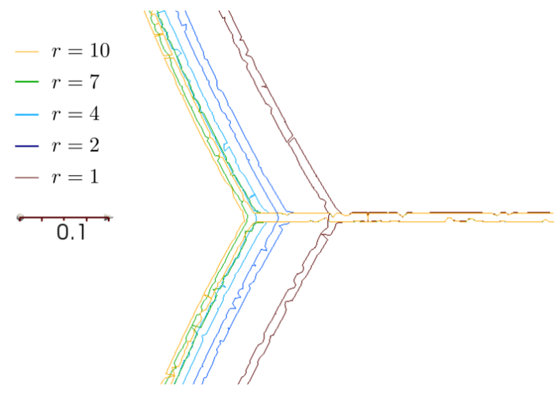

Fig. 12: Zoomed up image of the triple junction at t_{end} for different anisotropic ratios.

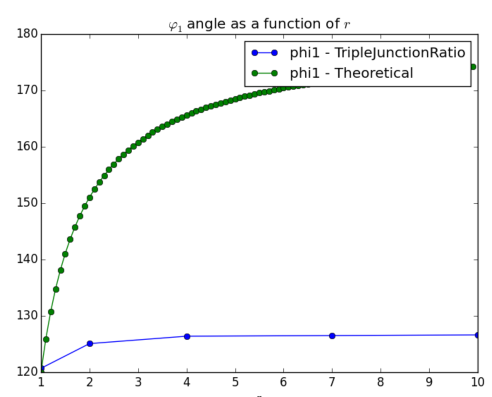

Fig. 13: Graph of φ_3 at t_{end} for different anisotropic ratios.

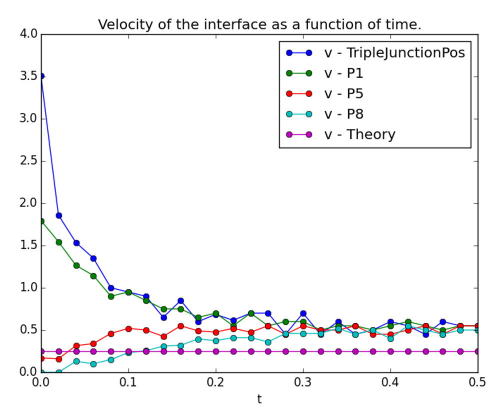

Fig. 14: Graph of v_x as a function of t for $r = 2$.

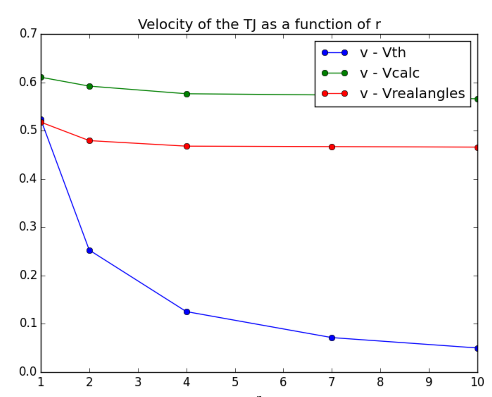

Fig. 15: Graph of v_x as a function of r, theoretical (blue), simulated (green) and with the obtained angles (red).

Varying Anisotropy

Equilibrium Angles

- As r increases, the solutions are closer and closer together.
- The angles for $r \neq 1$ are clearly much lower than predicted by the theory.
- Equation (9)/Young's equilibrium is not respected.
- Although convergence of the method is ensured, the simulation does not arrive at the correct solution.
- The question must be revisited in the state of the art.

Velocities

- Relative velocities of the triple junction get lower as r increases.
- A stationary state is obtained ($v_x = cnst$) for $t = 0.14$.
- Kinetics are around twice as fast as they should be for $r = 2$.
- Obtained velocities at the triple junction are much higher than those predicted using the imposed grain boundary energies for every $r \neq 1$.
- Kinetics of the triple junction are coherent with obtained angles.
- Kinetics of the profile completely dependent on the equilibrium angles.

Conclusions

- The equilibrium angles at the triple junction can not be obtained naturally without considering torque terms.
- The kinetics of the triple junction and its surroundings are completely dependent upon the equilibrium angles.

Bibliography

[BLC11] M. Bernacki, R.E. Logé, and T. Coupez. Level set framework for the finite-element modelling of recrystallization and grain growth in polycrystalline materials. *Scripta. Materialia*, 64:525–528, 2011.

[GNS99] Harald Garcke, Britta Nestler, and Barbara Stoth. A multi phase field concept: Numerical simulations of moving phase boundaries and triple junctions. *SIAM Journal of Applied Mathematics*, 1999.

[Her99] Conyers Herring. *Surface Tension as a Motivation for Sintering*. Springer Berlin Heidelberg, 1999.

[TCV16] Damien Texier, Jonathan Cormier, and Patrick Villechaise. Crack initiation sensitivity of wrought direct aged alloy 718 in the very high cycle fatigue regime: the role of non-metallic inclusions. *Material Science and Engineering*, 678:122–136, 2016.